A water-stable Eu^{III}-based MOF as a dual-emission luminescent sensor for discriminative detection of nitroaromatic pollutants

Xue-Jing Zhang, Fang-Zhe Su, Di-Ming Chen, Yu Peng, Wan-Ying Guo, Chun-Sen Liu* and Miao Du*

Henan Provincial Key Laboratory of Surface & Interface Science, Zhengzhou University of Light Industry, Zhengzhou 450002, P. R. China

Authors for correspondence: chunsenliu@zzuli.edu.cn; dumiao@zzuli.edu.cn

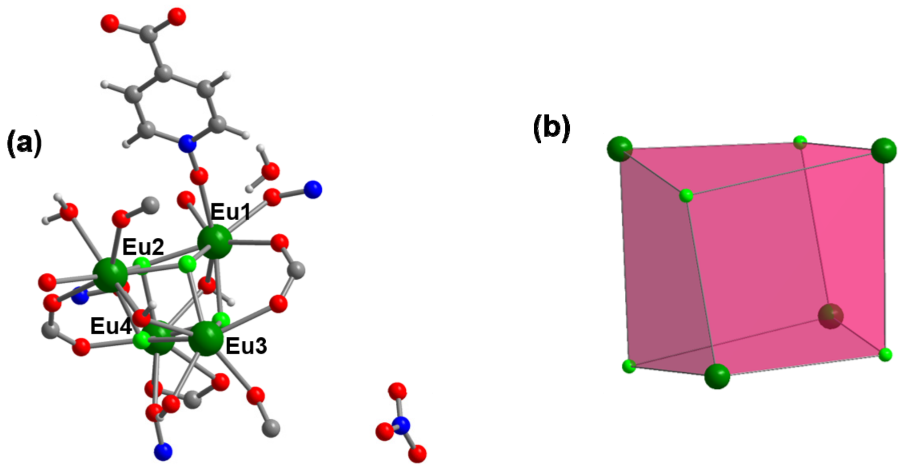

Fig. S1 (a) Coordination environments of Eu^{3+} centers; (b) The polyhedron formed by four Eu^{3+} centers and four Cl^{-} ions. Atom codes: Eu (green), C (gray), N (blue), O (red) and Cl (fluorescent green).

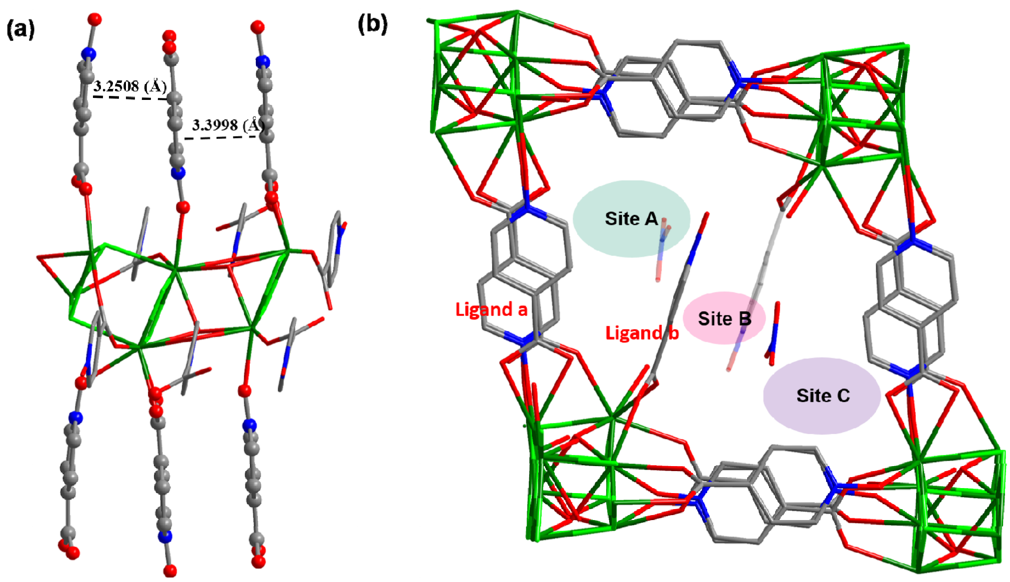

Fig. S2 Crystal structure of **Eu-MOF**. (a) The π–π interactions between the ligands; (b) A portion view of the channel. Site A is defined as slit-type pore between HINO and framework; Site B is defined as slit-type pore between HINO and NO_3^{-}; Site C is defined as slit-type pore between NO_3^{-} and framework.

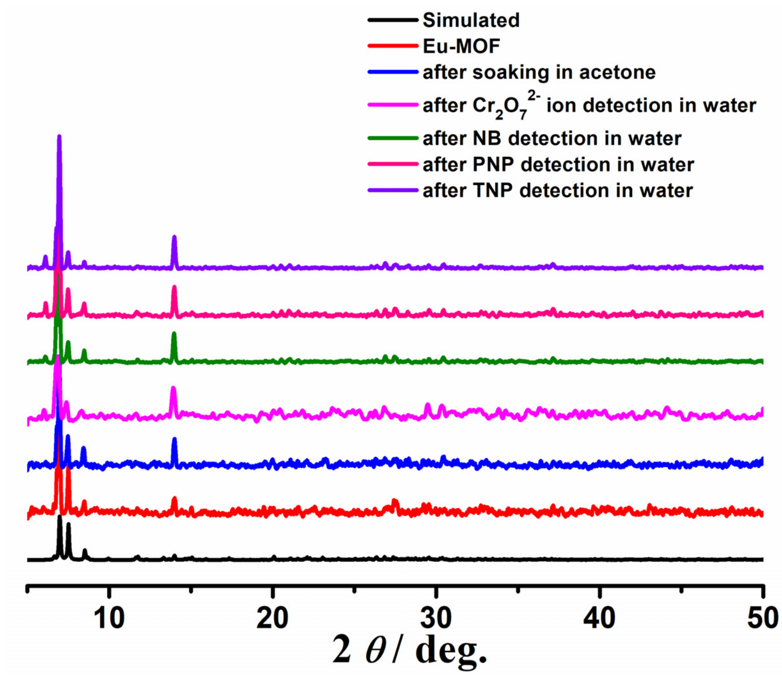

Fig. S3 PXRD patterns of **Eu-MOF** before and after detection.

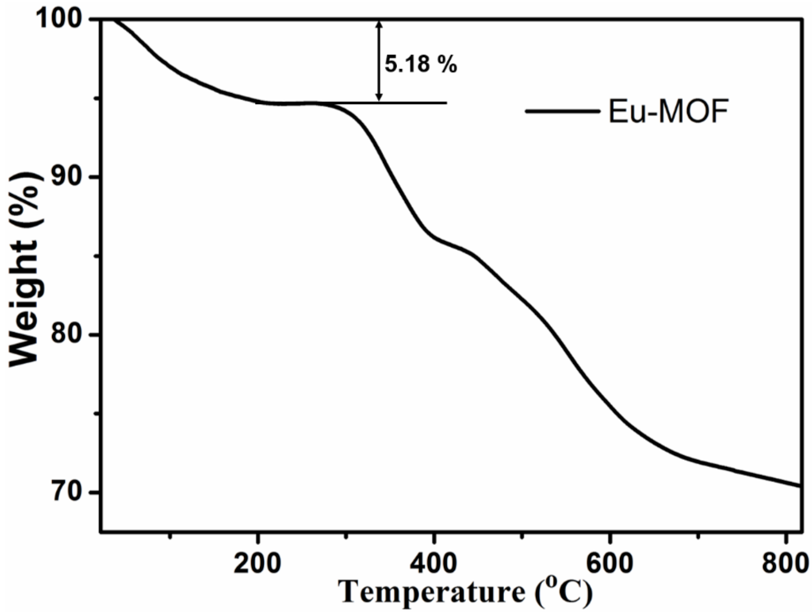

Fig. S4 Thermal gravimetric analysis (TGA) curve of **Eu-MOF**.

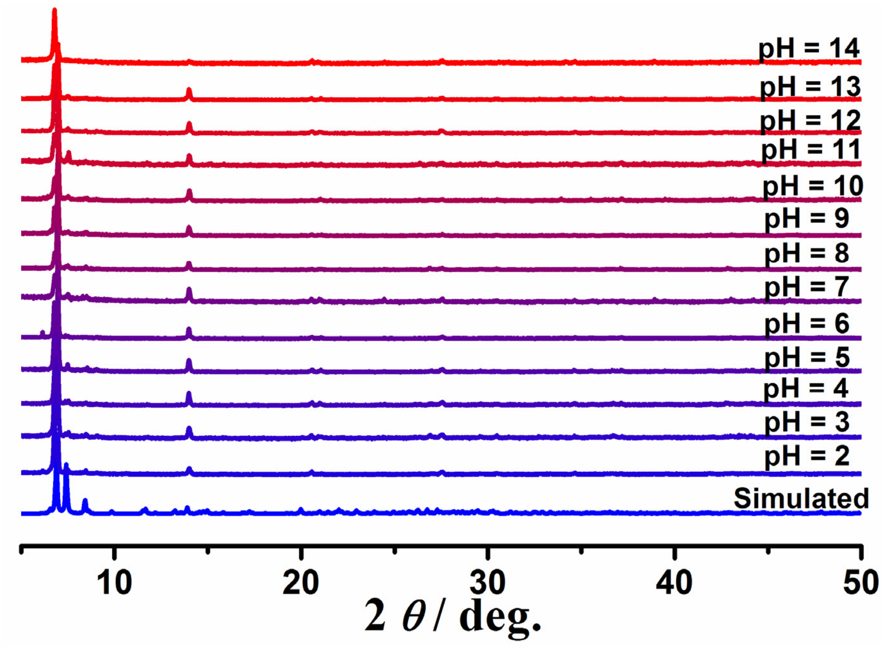

Fig. S5 PXRD patterns of **Eu-MOF** after immersing in water solutions with different pH values.

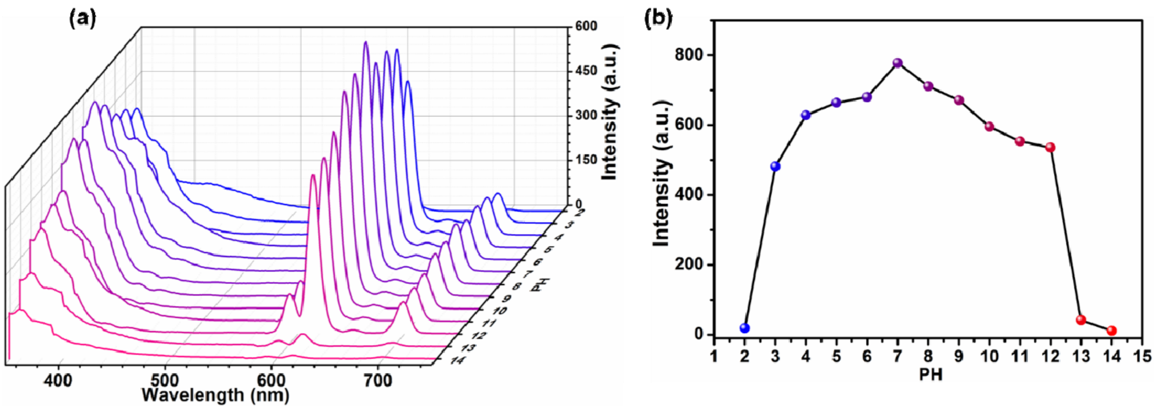

Fig. S6 Emission spectra (a) and emission intensities (b) of **Eu-MOF** in aqueous solutions with different pH values (2~14).

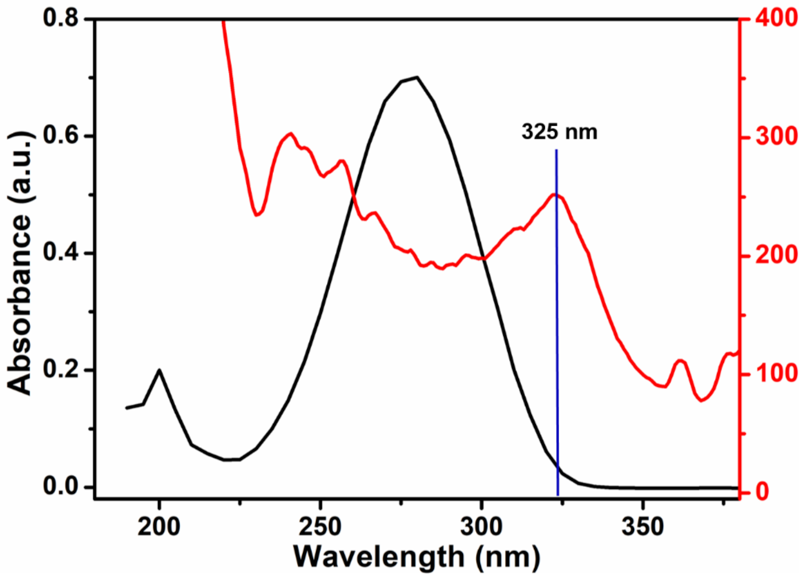

Fig. S7 UV adsorption spectrum of acetone (blank) and excitation spectrum of **Eu-MOF** (red).

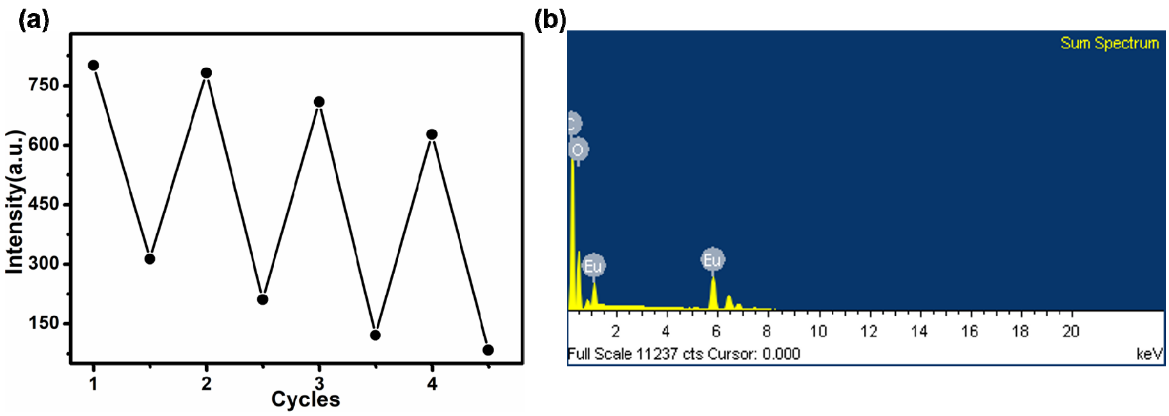

Fig. S8 (a) The quenching and recovery tests of **Eu-MOF** in $Cr_2O_7^{2-}$ solution; (b) The EDS spectrum of **Eu-MOF** after recyclable experiments for $Cr_2O_7^{2-}$ anion.

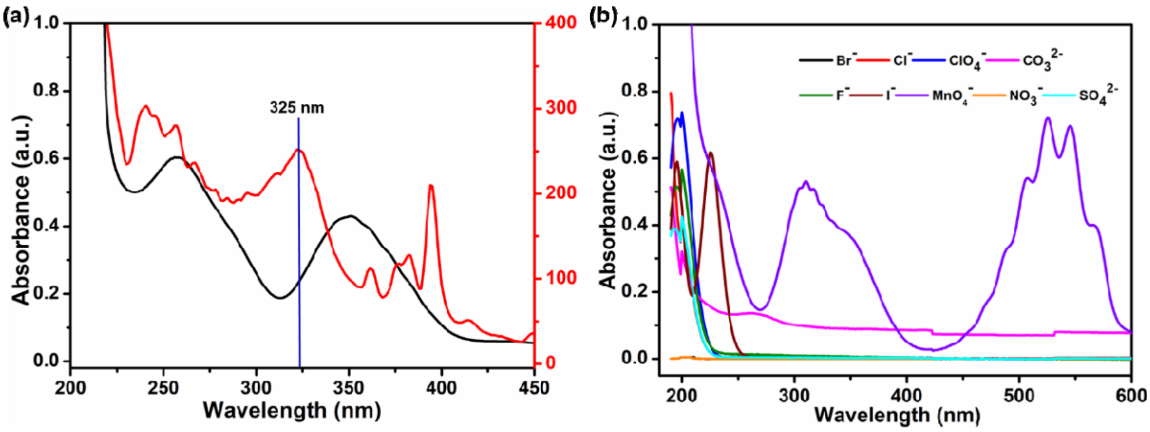

Fig. S9 (a) Exaction spectrum for **Eu-MOF** (red) and (b) UV adsorption spectra of aqueous solutions with testing anions (F^-, Cl^-, Br^-, I^-, NO_3^-, CO_3^{2-}, SO_4^{2-}, ClO_4^-, MnO_4^- and $Cr_2O_7^{2-}$).

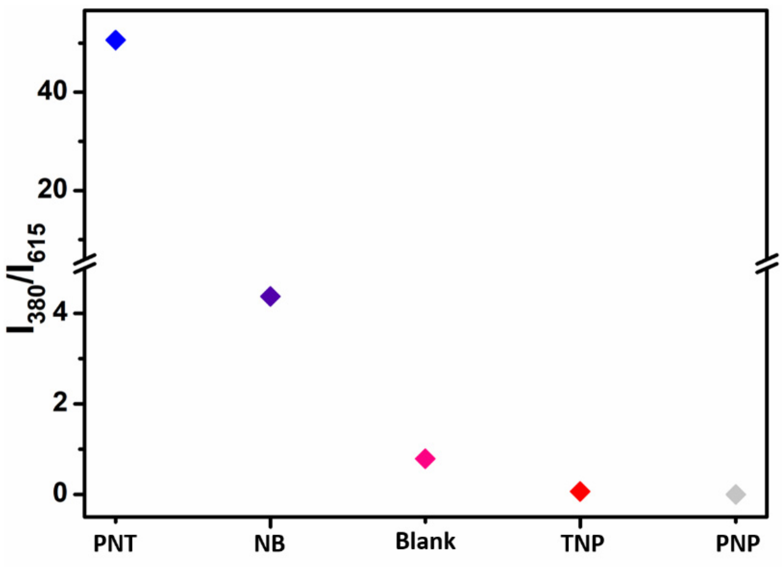

Fig. S10 The emission intensity ratios of the ligand (380 nm) to Eu^{3+} (615 nm) transitions with different NACs.

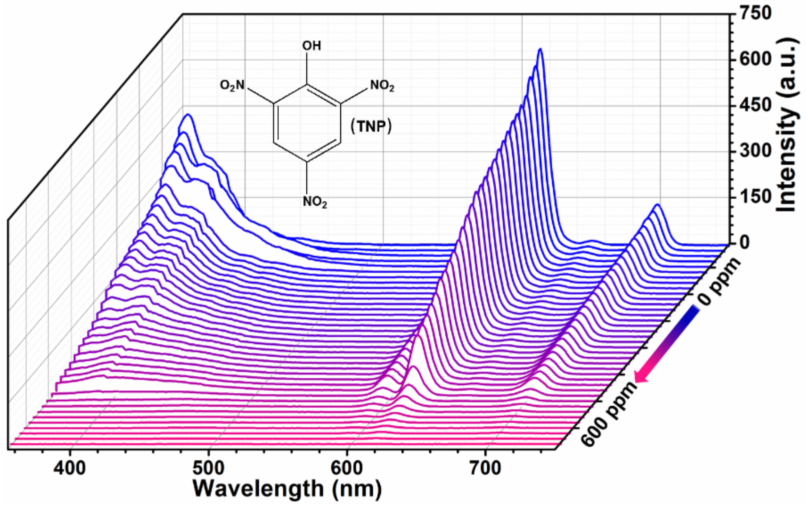

Fig. S11 Emission spectra of **Eu-MOF** in aqueous solutions with different concentrations of TNP.

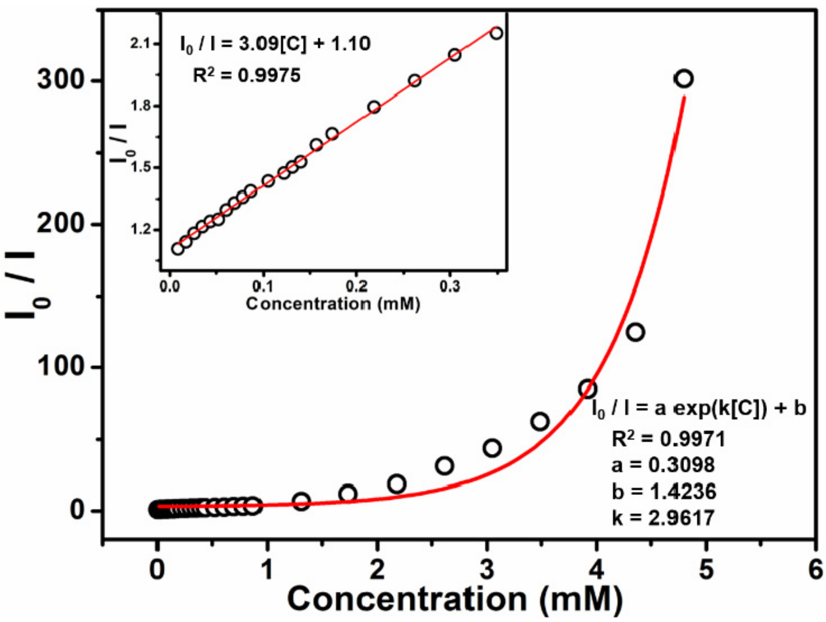

Fig. S12 SV plot of the **Eu-MOF** in aqueous solutions with different concentrations of TNP.

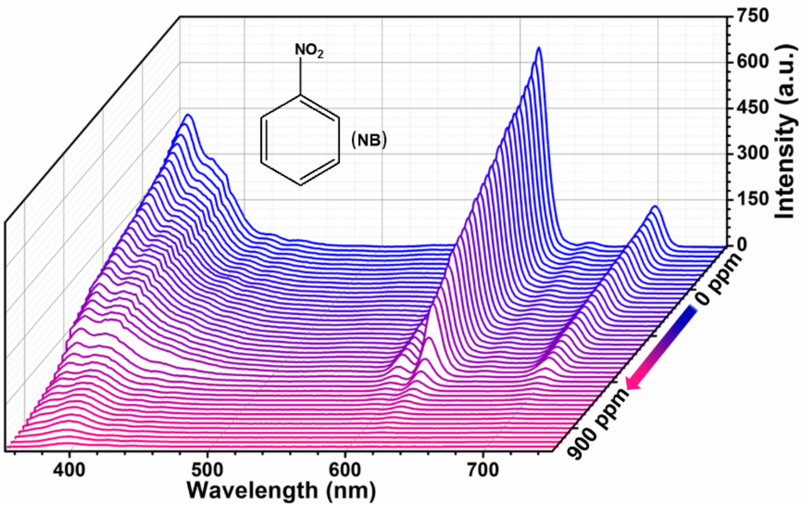

Fig. S13 Emission spectra of **Eu-MOF** in aqueous solutions with different concentrations of NB.

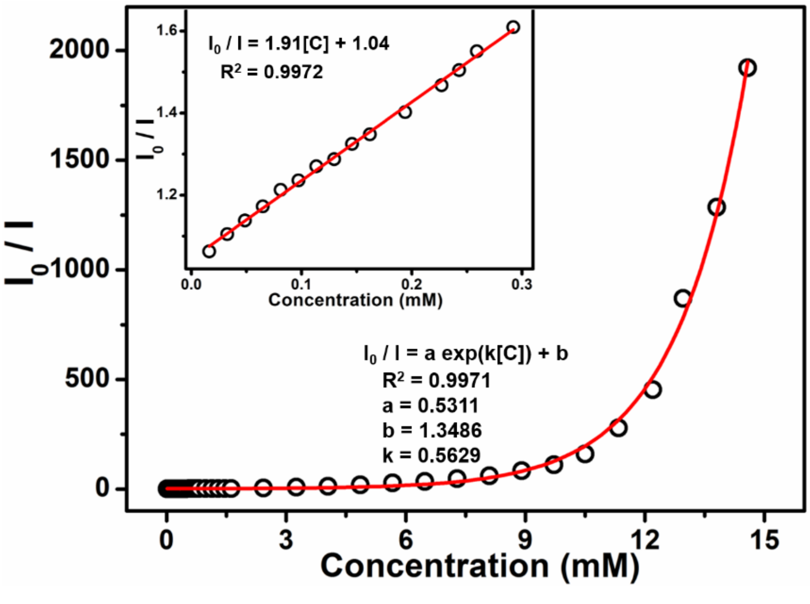

Fig. S14 SV plot of **Eu-MOF** in aqueous solutions with different concentrations of NB.

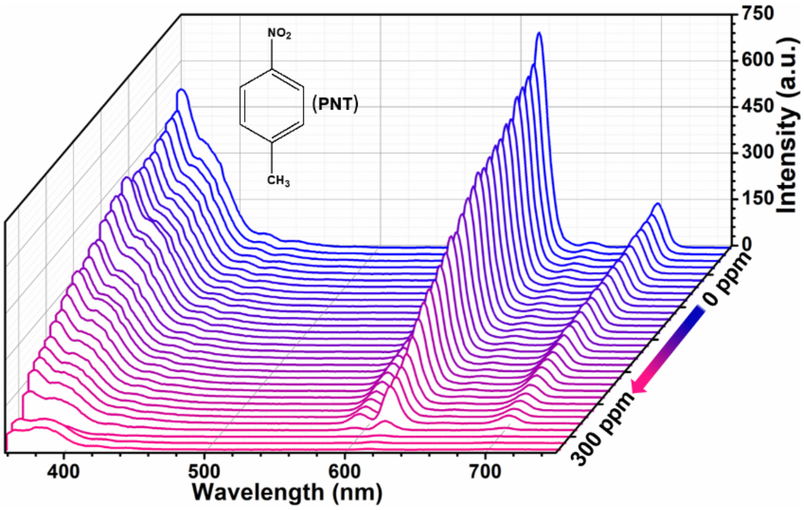

Fig. S15 Emission spectra of **Eu-MOF** in aqueous solutions with different concentrations of PNT.

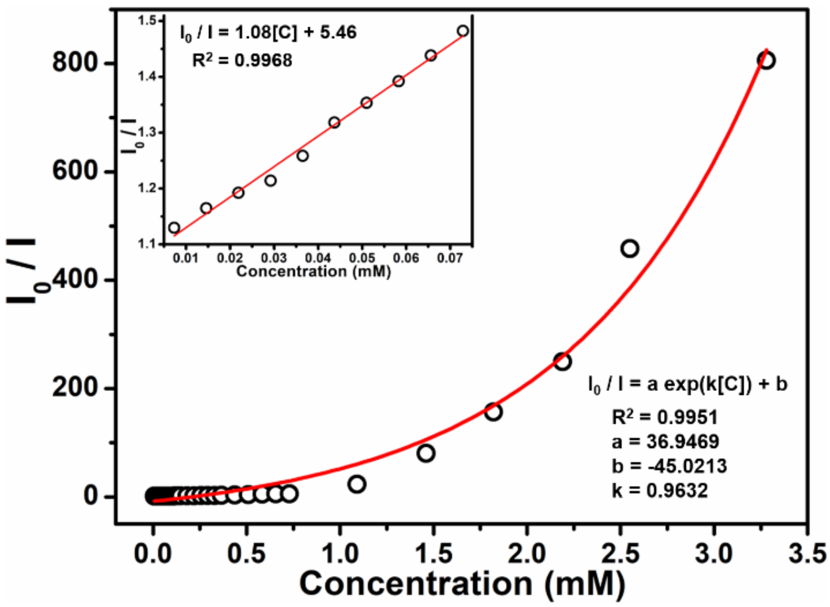

Fig. S16 SV plot of **Eu-MOF** in aqueous solutions with different concentrations of PNT.

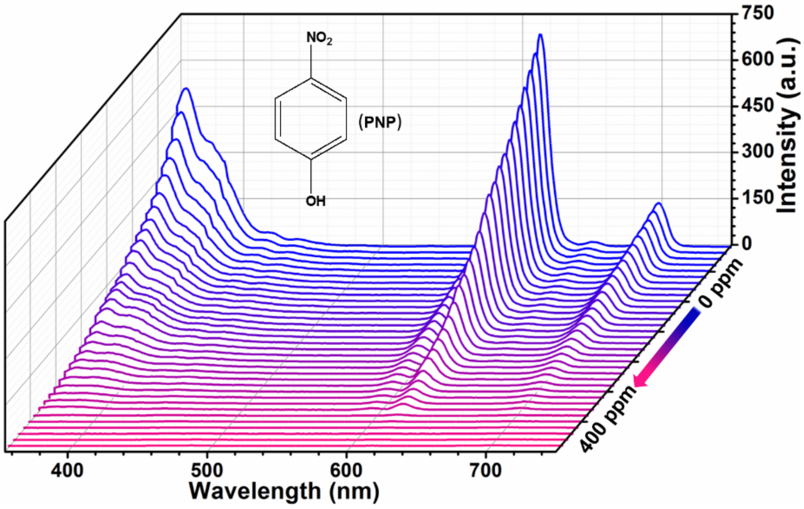

Fig. S17 Emission spectra of **Eu-MOF** in aqueous solutions with different concentrations of PNP.

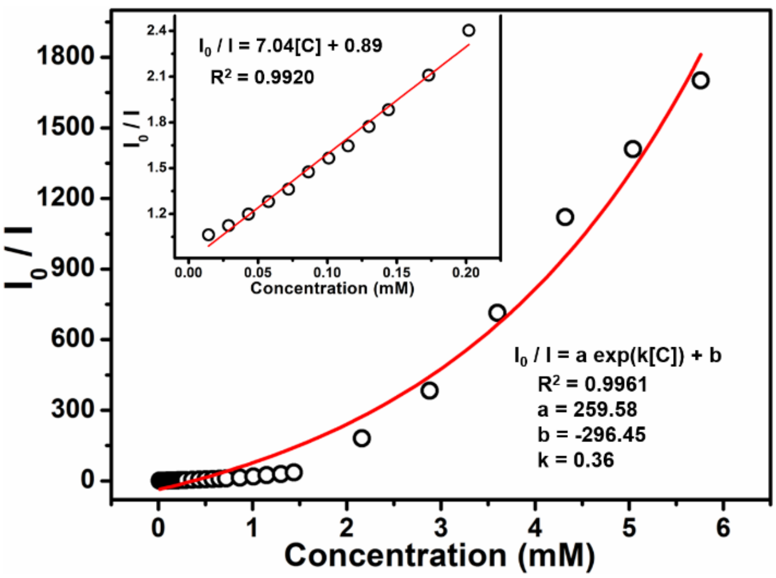

Fig. S18 SV plot of **Eu-MOF** in aqueous solutions with different concentrations of PNP.

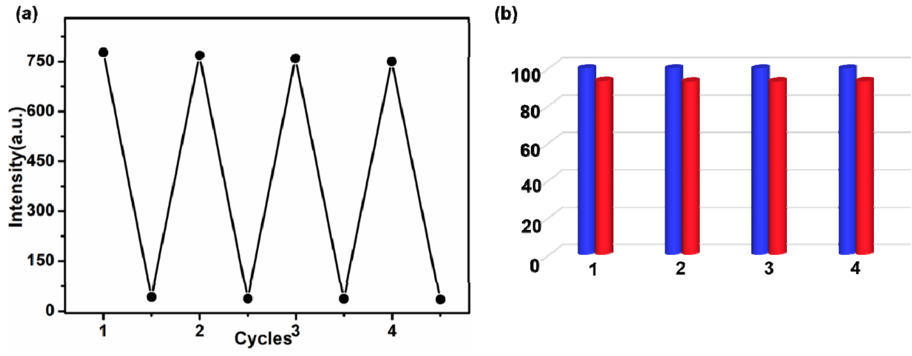

Fig. S19 Quenching efficiencies of **Eu-MOF** in recyclable experiments for TNP.

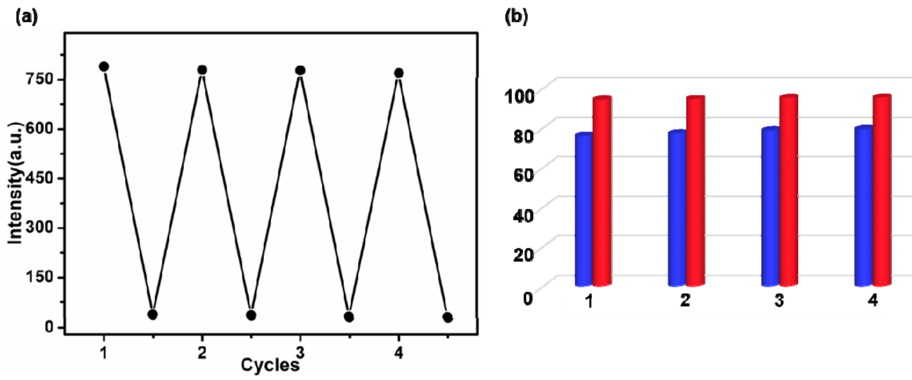

Fig. S20 Quenching efficiencies of **Eu-MOF** in recyclable experiments for NB.

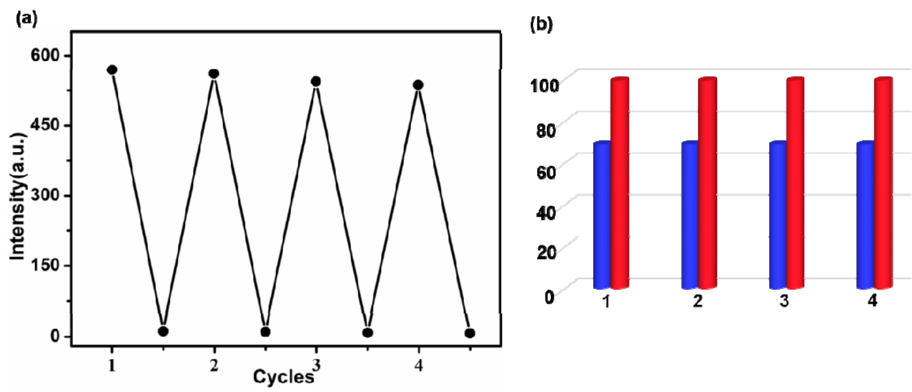

Fig. S21 Quenching efficiencies of **Eu-MOF** in recyclable experiments for PNT.

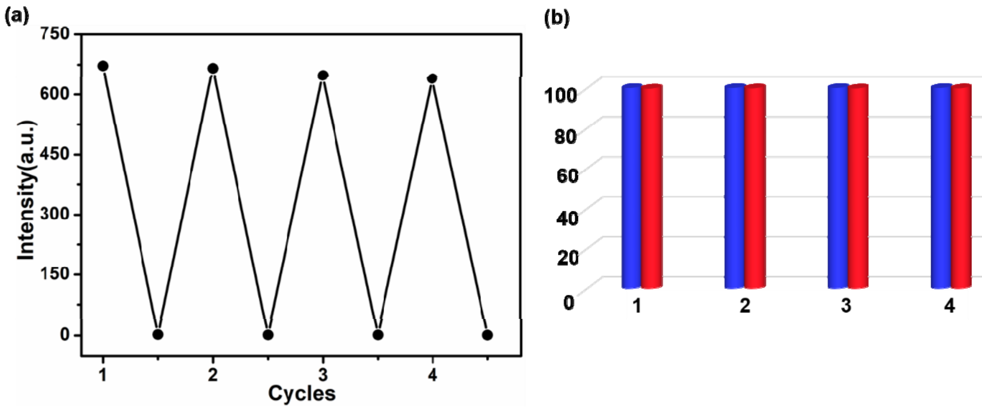

Fig. S22 Quenching efficiencies of **Eu-MOF** in recyclable experiments for PNP.

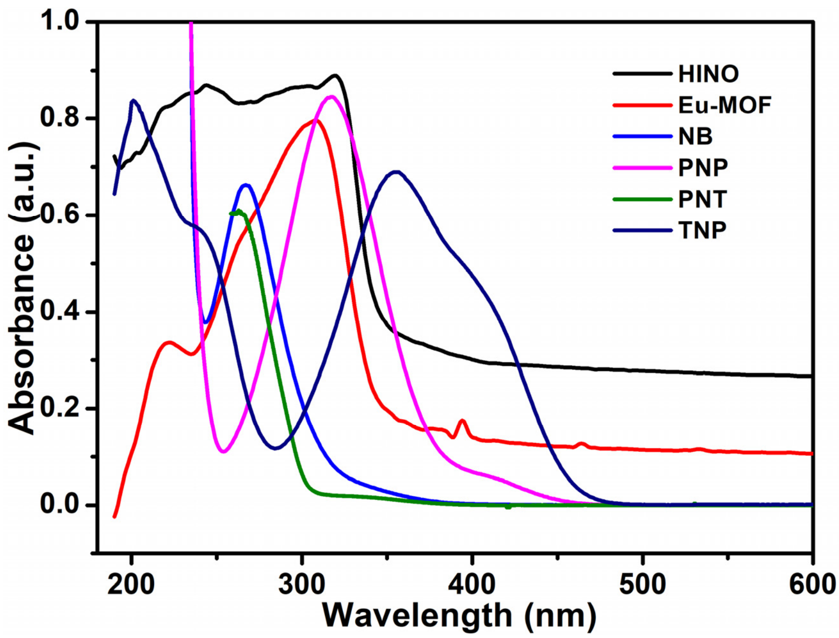

Fig. S23 UV adsorption spectra of aqueous solutions of nitroaromatic compounds (TNP, NB, PNT, and PNP) in water and exaction spectra for the ligand and **Eu-MOF**.

Table S1 Selected crystallographic parameters of **Eu-MOF**

	Eu-MOF
Formula	$C_{60}H_{68}Cl_8Eu_8N_{12}O_{52}$
Fw	3288.57
Cryst size, mm	0.24 / 0.11 / 0.05
Temp, K	293(2)
Crystal syst	triclinic
Space group	*P*-1
a, Å	12.7715(14)
b, Å	13.3164(13)
c, Å	13.7049(12)
α, deg	89.617(7)
β, deg	76.348(9)
γ, deg	72.055(9)
V, Å^3	2149.3(4)
Z	1
Dc, g cm^{-3}	2.415
μ, mm^{-1}	6.094
F(000)	1478
GOF on F^2	1.123
R_1, wR_2 [$I > 2\sigma(I)$]	0.0606, 0.1556
R_1, wR_2 (all data)	0.0744, 0.1643
Max / min, e Å^{-3}	2.234 / −2.364